21. L. R. Faulkner, A. J. Bard, in *Electroanalytical Chemistry*, A. J. Bard, Ed. (Dekker, New York, 1977), vol. 20, pp. 1–95.
22. T. C. Richards, A. J. Bard, *Anal. Chem.* **67**, 3140 (1995).
23. H. S. White, A. J. Bard, *J. Am. Chem. Soc.* **104**, 6891 (1982).
24. A. W. Knight, G. M. Greenway, *Analyst* **119**, 879 (1994).
25. M. Shim, P. Guyot-Sionnest, *Nature* **407**, 981 (2000).
26. C. Wang, M. Shim, P. Guyot-Sionnest, *Science* **291**, 2390 (2001).
27. T. Makimura, Y. Kunii, N. Ono, K. Murakami, *Appl. Surf. Sci.* **127–129**, 388 (1998).
28. H. C. Choi, J. M. Buriak, *Chem. Mater.* **12**, 2151 (2000).
29. The support of this research by grants from NSF and the Robert A. Welch Foundation is gratefully acknowledged. Thanks to P. Barbara, F. R. Fan, and M. Buda for helpful discussions.

26 December 2001; accepted 3 April 2002

Global Azimuthal Anisotropy in the Transition Zone

Jeannot Trampert[1]* and Hendrik Jan van Heijst[2]

Surface wave dispersion measurements for Love wave overtones carry evidence of azimuthal anisotropy in the transition zone of Earth's mantle (400 to 660 kilometers deep). A Backus-Gilbert inversion of anisotropic phase velocity maps, with resolution kernels mainly sensitive to the transition zone, shows a robust long-wavelength azimuthally anisotropic velocity structure. This observation puts new constraints on the mineralogy and dynamics of the transition zone because this anisotropy may result from aligned minerals, tilted laminated structures, or even organized pockets of fluid inclusions.

The nature of the transition zone has always been central to understanding the dynamics of Earth's mantle. Our inferences on the thermal and chemical evolution of Earth depend largely on whether the transition zone is due to pressure-induced phase changes and/or compositional variations of minerals (*1*). All seismic investigations of transition zone structure assume isotropic velocities. Seismic anisotropy is recognized as a good indicator of deformation and mantle flow (*2*, *3*), but is mainly observed in the uppermost mantle (*4*). Particularly in the transition zone, the observation of anisotropy is difficult because fundamental mode surface waves have most of their sensitivity above the transition zone and the bulk of teleseismic body waves, below. Nevertheless, an indication of radial anisotropy around the 660-km discontinuity was found by reconciling observations of body wave travel times and free oscillation frequencies with a spherically symmetric model (*5*). Indications of localized azimuthal anisotropy near the same depth are inferred from compressional (P) to horizontal shear (SH) wave conversions (*6*, *7*). Some observations of mainly S wave splitting require anisotropy in the upper transition zone (400 to 520 km) (*8*) and just below the 660-km discontinuity (*9*).

It recently became possible to make automatic surface wave overtone phase velocity measurements from millions of seismograms (*10*). These data are ideally suited for studying the transition zone because of their peak sensitivity in this depth range. Theory indicates (*11*, *12*) that a slightly anisotropic medium causes an azimuthal dependence of local phase velocities of Love and Rayleigh surface waves as follows

$$\frac{dc}{c}(\omega,\psi) = \alpha_0(\omega) + \alpha_1(\omega)\cos(2\psi) + \alpha_2(\omega)\sin(2\psi) + \alpha_3(\omega)\cos(4\psi) + \alpha_4(\omega)\sin(4\psi) \quad (1)$$

where dc/c is the relative phase velocity perturbation with respect to a spherically symmetric reference Earth model, ω is the radial frequency, and ψ is the azimuth along the path. It can be shown that the $\alpha_i(\omega)$ are local vertical averages of 13 independent linear combinations of specific elements of the stiffness tensor (*13*). $\alpha_0(\omega)$ corresponds to the average over all azimuths and describes transverse or radial anisotropy involving the well-known Love parameters A, C, F, L, and N (*14*). The 2ψ and 4ψ terms involve an additional eight parameters that describe the azimuthal variations of A, F, L, and N. To make robust inferences of anisotropy, we chose to use Love wave overtones only [see Methods in Supporting Online Material (SOM)], where the 2ψ and 4ψ terms depend on one elastic parameter each, referred to as G and E, respectively (*13*).

We selected more than 100,000 Love wave measurements for minor and major arc paths corresponding to the first and second overtone branch (see Methods in SOM). The minor arc is the great circle angular distance between source and receiver, and the major arc is its complement. The path averaged phase velocity measurements are used to derive models of azimuthal anisotropy specified by the coefficients $\alpha_i(\omega)$ (see Methods in SOM). Fundamental mode phase data cannot easily distinguish between isotropic and anisotropic models (*15*, *16*) because of the uneven local azimuthal coverage, which is responsible for tradeoffs between the different $\alpha_i(\omega)$. We designed a technique based on relative weighting, which finds the optimal amount of azimuthal anisotropy for a given data set (see Methods in SOM), and we constructed phase velocity models based on Eq. 1. Toroidal overtone measurements are more difficult to make than spheroidal ones and have not previously been used for inferring three-dimensional (3D) Earth structure. Apart from strict quality checks on the data (*17*), the original measurement technique (*10*) has been extend to major arcs, which makes the overtone separation easier due to a longer distance of propagation. We further compared the isotropic part of our constructed phase velocity maps with those predicted from the 3D velocity model S20RTS (*18*). This model did not use any Love wave data, and the predictions can thus be used as an independent quality check of our measurements. For all selected overtones, the correlation (up to spherical harmonic degree 20) between our $\alpha_0(\omega)$ maps and the S20RTS predictions ranged from 0.75 to 0.80 with bootstrap confidence levels (*19*) higher than 99%. These high correlations corroborate the effectiveness of the measuring technique to separate overtones.

The anisotropic phase velocity models specify at each point on Earth's surface the local depth averages of the anisotropic parameters G and E that describe the 2ψ variation of the vertical shear velocity (SV) and the 4ψ variation of the SH velocity, respectively. The depth kernels are calculated in a spherical Earth (*16*, *20*) (fig. S1). At a given depth, G and E are calculated from the secondary data $[\alpha_i(\omega)]$ and the kernels. This represents a linear inverse problem, and the most general solution is to construct models as a linear combination of the data themselves. We opted for a Backus-Gilbert approach (*21*), where the resolution of the model itself is optimized toward a desired shape (see Methods in SOM). For our given overtones, we were able to find a set of coefficients that give resolution kernels mainly sensitive to the transition zone (Fig. 1). These resolution kernels show that most structure above and below the transition zone cancels out; i.e., a synthetic test with data derived from a target model above or below the transition zone would retrieve an almost zero model, whereas a target in the transition zone would be fully recovered. Such a Backus-Gilbert inversion represents a test of whether or not anisotropy is present in the transition zone.

[1]Faculty of Earth Sciences, Utrecht University, Post Office Box 80021, 3508 TA Utrecht, Netherlands. [2]Shell International Exploration and Production, Post Office Box 60, 2280 AB Rijswijk, Netherlands.

*To whom correspondence should be addressed. E-mail: jeannot@geo.uu.nl.

The horizontal resolution is determined by the resolution of the individual phase velocity maps (fig. S2). It differs slightly for each overtone because the ray coverage is not exactly the same. This could introduce spurious structure in the target zone because we take a linear combination of phase velocities with varying spatial resolution. The resolution of the lowest spherical harmonic degrees is equal for all phase velocity maps because we made unbiased, low-degree expansions. For robustness, we concentrated on degree 2 for the 2ψ maps and degree 4 for the 4ψ maps. All the variance reduction gained by the introduction of azimuthal terms in the phase velocity maps (1.5 to 2% per overtone, fig. S3) can potentially be put into the target zone by the Backus-Gilbert technique and bias the amplitude estimation. Love wave overtones are strongly sensitive to the G parameter, which allowed us to design an experiment to constrain the amplitude in the inversion. Fundamental mode surface wave dispersion is easier to measure, and we constructed azimuthally anisotropic phase velocity maps for 100-s Rayleigh waves using 75,515 minor and major arc measurements. We then chose the Backus-Gilbert target to be the sensitivity kernel for the G parameter of this fundamental mode Rayleigh wave (Fig. 1). The coefficients for the linear combination that matches the target were obtained, solving an optimization problem that needs regularization. Damping was chosen so that the root mean square (rms) amplitudes in both maps were similar. This damping, which can be used for all inversions with the same data, has a direct influence on the amplitude match but not on the directions that remain unchanged for large ranges of damping. This suggests that the anisotropic directions are robust. The overall correspondence is very good (Fig. 2, fig. S4A), giving a correlation between the two G fields of 0.7 with a bootstrap confidence level higher than 99%. Remaining differences may be due to the elastic constants B and H (with strong sensitivity to lithospheric structure), which contribute to the fundamental mode Rayleigh wave map, but we cannot model with Love wave overtones. Another concern could be the influence of topography on existing seismic discontinuities. We performed a test correcting the measured Love wave overtone phase velocities with crustal model CRUST5.1 (*22*) before inversion. This left the azimuthal terms unchanged, indicating a low trade-off between crustal thickness and the azimuthal terms. Because the topography on the Moho depth is probably larger than any topography on the 400- and 660-km discontinuities, we suggest that undulations on seismic discontinuities have at most a second order influence on our modeled azimuthal anisotropy.

The results for the transition zone anisotropy (Fig. 3) show lateral variations of G with a rms amplitude of 1%. This is about three times as large as the rms amplitude for E. Given the sensitivity of our overtones, we can change the position of the target zone to get anisotropic models at different depths. Between 100 to 200 km depth, the rms amplitude of the G parameter is 0.5% and decreases to 0.2% between 200 and 400 km. In the transition zone, amplitudes increase again. The overall 2ψ correlation between the transition zone model (Fig. 3B) and our predicted surface model (Fig. 2B) is -0.55 with a bootstrap confidence level of just under 80%. The negative sign indicates an anticorrelation between models close to the surface and those in the transition zone, but plotting local differences of directions on the sphere (fig. S4B) shows a more complex pattern than a simple 90° rotation. The E parameter has a rms amplitude of 0.6% between 100 and 200 km depth and decreases to a constant level of 0.3% in deeper parts of the upper mantle. Worrisome could be the possible coupling of modes, which could alter the sensitivity kernels. The linear combination of overtones we deduced from the uncoupled kernels, then, would not necessarily eliminate structure outside the transition zone. Along-branch coupling is not an issue, because the kernels vary smoothly with frequency for a given overtone. Cross-branch coupling is possible (*23*), but no detailed study has been done on how strong coupling might be for an arbitrary stiffness tensor. Our Rayleigh prediction (Fig. 2) might help assess this question. The self-coupling Love wave overtone kernels, as used here, cannot predict azimuthal anisotropy

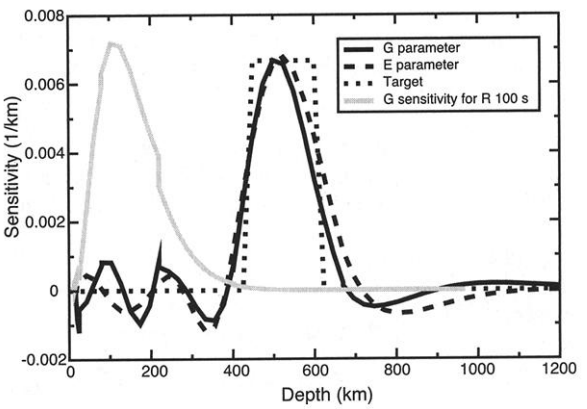

Fig. 1. Backus-Gilbert averaging kernels. The Backus-Gilbert inversion seeks coefficients for the linear combination of overtones necessary to achieve the target resolution in the transition zone. Shown are the resulting resolution kernels for parameters G and E. The side lobes are fairly minor because the target zone is wide. Also shown is the sensitivity kernel for the G parameter of a fundamental mode Rayleigh wave at 100 s.

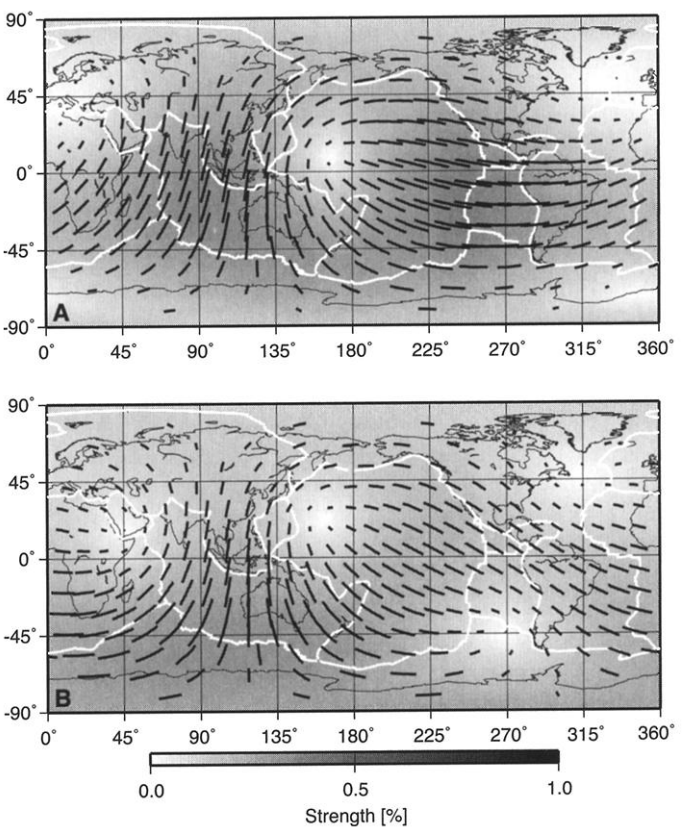

Fig. 2. Comparison of independently observed (**A**) and predicted (**B**) 2ψ terms. (A) The observed field corresponds to the 100-s fundamental mode Rayleigh wave phase velocity model, and (B) the predicted field is obtained from Love wave overtones using our Backus-Gilbert approach. The gray scale in the background corresponds to the peak-to-peak amplitude of anisotropy expressed relative to the average phase velocity calculated from the Preliminary Reference Earth Model (PREM) (*30*). The black lines represent the fast directions, which are also scaled relative to the amplitude of anisotropy shown in the background. The plate boundaries are plotted in white.

observed from fundamental mode Rayleigh waves if the kernels are strongly affected by cross-branch coupling. The presence of possible higher degree structure and a more classical inversion for a full model might change some details of our observations, but our analyses shows that transition zone anisotropy is required by the seismic data. This anisotropy remained undetected for so long because long-period fundamental mode Love waves, though sensitive to the transition zone, show little sensitivity to G, and E has a small amplitude in the transition zone. Long-period Rayleigh waves suffer from tradeoff between G, B, and H are thus difficult to analyze. Only Love wave overtones have the right sensitivity to G and E in the transition zone.

This observation of anisotropy puts constraints on the nature of the transition zone. Both the lattice-preferred orientation (LPO) of anisotropic minerals and the shape-preferred orientation (SPO) of secondary phases can give rise to anisotropic structures in Earth's mantle. The occurrence of these structures depends on the deformation mechanism in the mantle. Dislocation creep is generally favored in boundary layers, which can result in LPO and SPO (*24*), but SPO obtained by diffusion creep cannot be excluded as yet. Candidates for LPO are wadsleyite and ringwoodite, anisotropic crystals resulting from phase transitions of olivine in the transition zone (*25*). Depending on the geotherm and aluminum content in the upper mantle, ilmenite is another strongly anisotropic crystal that could be present. To explain observed transverse anisotropy in and below the transition zone, Karato (*24*) favors laminated structures (SPO). If these structures are tilted, azimuthal anisotropy could result. SPO of partial melt inclusions has been evoked to explained observed anisotropy in the lowermost mantle (*26*), but the presence of partial melt in the transition zone is not as likely (*27*). Assuming that dislocation creep is responsible for our observations, one is tempted to infer that mantle flow should have some horizontal component in the transition zone. However, recent modeling efforts (*28*) and experiments on wet olivine (*29*) showed that the correspondence between flow geometry and fast anisotropic directions is more complicated than previously thought.

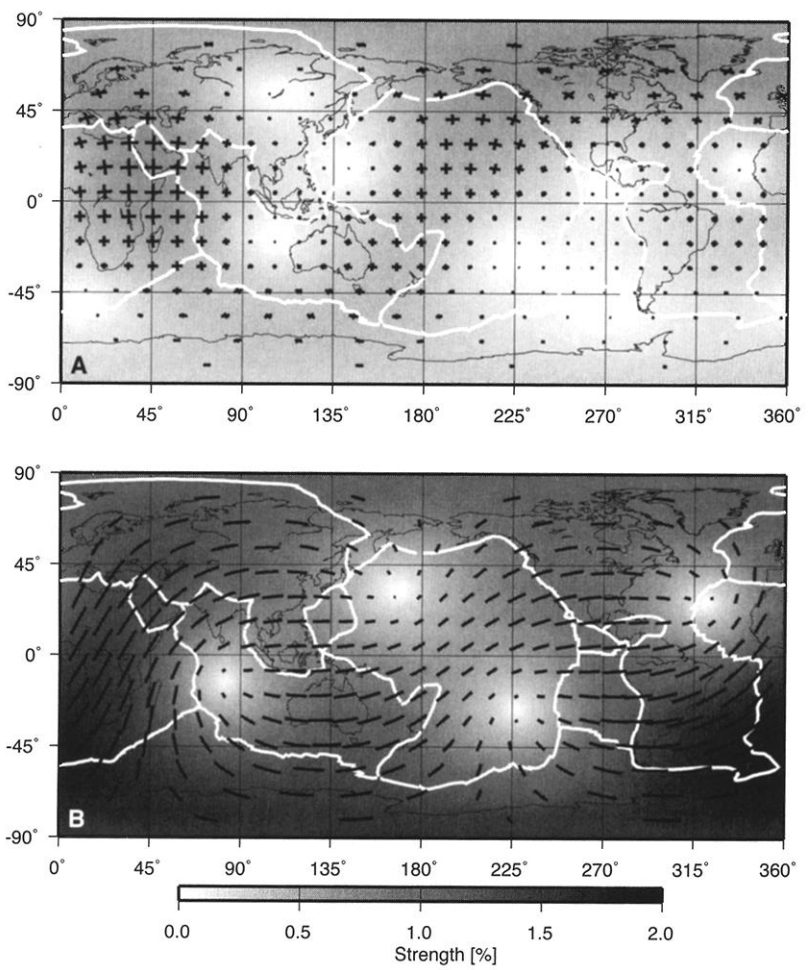

Fig. 3. The transition zone model for E (**A**) and G (**B**) corresponding to the resolution kernels in Fig. 1. The gray scale in the background corresponds to the peak-to-peak amplitude of anisotropy expressed relative to the average elastic Love parameter L of PREM. The black lines represent the fast directions, and the plate boundaries are in white.

References and Notes

1. G. F. Davies, *Dynamic Earth: Plates, Plumes and Mantle Convection* (Cambridge Univ. Press, Cambridge, 1999).
2. S. Karato, in *Seismic Anisotropy: Mechanisms and Tectonic Implications*, S. Karato, M. Toriumi, Eds. (Oxford Univ. Press, Oxford, 1989), pp. 393–422.
3. J.-P. Montagner, *Rev. Geophys.* **32**, 115 (1994).
4. ———, *Pure Appl. Geophys.* **151**, 223 (1998).
5. ———, B. L. N. Kennett, *Geophys. J. Int.* **125**, 229 (1996).
6. L. Vinnik, J.-P. Montagner, *Geophys. Res. Lett.* **23**, 2449 (1996).
7. L. Vinnik, S. Chevrot, J.-P. Montagner, *Geophys. Res. Lett.* **25**, 1995 (1998).
8. M. J. Fouch, K. M. Fischer, *J. Geophys. Res.* **101**, 15987 (1996).
9. J. Wookey, J.-M. Kendall, G. Barruol, *Nature* **415**, 777 (2002).
10. H. J. van Heijst, J. H. Woodhouse, *Geophys. J. Int.* **131**, 209 (1997).
11. M. L. Smith, F. A. Dahlen, *J. Geophys. Res.* **78**, 3321 (1973).
12. ———, *J. Geophys. Res.* **80**, 1923 (1975).
13. J.-P. Montagner, H.-C. Nataf, *J. Geophys. Res.* **94**, 295 (1986).
14. E. H. Love, *A Treatise on the Theory of Elasticity* (Cambridge Univ. Press, Cambridge, ed. 4, 1927).
15. G. Laske, G. Masters, *Geophys. J. Int.* **132**, 508 (1998).
16. E. W. F. Larsen, J. Tromp, G. Ekström, *Geophys. J. Int.* **132**, 654 (1998).
17. H. J. van Heijst, J. H. Woodhouse, *Geophys. J. Int.* **137**, 601 (1999).
18. J. Ritsema, H. J. van Heijst, J. H. Woodhouse, *Science* **286**, 1925 (1999).
19. B. Efron, R. Tibshirani, *Science* **253**, 390 (1991).
20. B. Romanowicz, R. Snieder, *Geophys. J. R. Astron. Soc.* **93**, 91 (1988).
21. G. Backus, F. Gilbert, *Geophys. J. R. Astron. Soc.* **16**, 169 (1968).
22. W. D. Mooney, G. Laske, G. Masters, *J. Geophys. Res.* **103**, 727 (1998).
23. J. Park, *Geophys. J. Int.* **129**, 399 (1997).
24. S. Karato, *Pure Appl. Geophys.*, **151**, 565, (1998).
25. D. Mainprice, G. Barruol, W. Ben Ismaïl, in *Earth's Deep Interior: Mineral Physics and Tomography From the Atomic to the Global Scale*, S. Karato, A. Forte, R. Liebermann, G. Masters. L. Stixrude, Eds. (Geophysical Monograph 117, American Geophysical Union, Washington, 2000), pp. 237–264.
26. J.-M. Kendall, in *Earth's Deep Interior: Mineral Physics and Tomography From the Atomic to the Global Scale*, S. Karato, A. Forte, R. Liebermann, G. Masters, L. Stixrude, Eds. (Geophysical Monograph 117, American Geophysical Union, Washington, 2000). pp. 133–159.
27. R. Boehler, *Philos. Trans. R. Soc. London Ser. A* **354**, 1265 (1996).
28. P. R. Dawsen, H.-R. Wenk, *Philos. Mag. A* **80**, 573 (2000).
29. H. Jung, S. Karato, *Science* **293**, 1460 (2001).
30. M. Dziewonski, D. L. Anderson, *Phys. Earth Planet. Int.* **25**, 297 (1981).

31. J. Woodhouse provided the code for calculating the path averaged generalized spherical harmonics. J.T. gratefully acknowledges a visiting professorship at Ecole Normale Supérieure in Lyon, where discussions with Y. Ricard inspired the Backus-Gilbert approach. S. Karato and an anonymous reviewer provided helpful comments.

Supporting Online Material

(www.sciencemag.org/cgi/content/full/296/5571/1297/DC1)

Methods

figs. S1 through S4

25 January 2002; accepted 3 April 2002